*Geophys. J. R. astr. Soc.* (1976) **44**, 177–201

# Some Numerical Solutions for Turbulent Boundary-Layer Flow above Fixed, Rough, Wavy Surfaces

**P. A. Taylor, P. R. Gent and J. M. Keen**

(Received 1975 June 17)*

*Summary*

Flow in a deep turbulent boundary-layer above a rough, rigid, wavy surface is considered. Closure is made via mixing-length hypotheses and at the level of the turbulent energy equation and the resulting equations are solved numerically using finite difference approximations. Results are presented for a typical case representative of flow above gravel waves on the bed of a tidal channel and the effect of changes in wave amplitude, shape and surface roughness are considered. Comparisons are made with recent experimental and theoretical studies. In some computations allowance is made for the effect of streamline curvature on the turbulence structure and the importance of such effects for these flows is assessed.

## 1. Introduction

There are many situations in micrometeorology and oceanography where it would be helpful if we knew a little more about the behaviour of turbulent boundary-layers above non-plane surfaces. Examples are the flow of water over sand or gravel waves, the flow of air above wind waves, or, on land, over small ridges and other topographic features. If the surface topography has a length scale which is large compared to the depth of the boundary-layer then we have the classic situation in which the horizontal pressure gradients within the boundary-layer and the flow outside it are determined by the potential flow solution for inviscid irrotational flow over the topography in question. This approach has been used by Hino (1968) for flow in the atmospheric boundary-layer while, for example, Paskonov & Soprunenko (1963) have used the method in a study of the laminar boundary-layer on a wavy wall. In many instances however the horizontal length scales of the topography are of the same order of magnitude as the depth of the boundary-layer and, if we wish to study flow over such features then a straightforward boundary-layer approximation will not be applicable. Under these circumstances we must seek solutions to the flow in which ' dynamic pressure ' effects are retained within the boundary-layer. This step has been taken by several workers in atmospheric situations, for example Onishi & Estoque (1968) and Shir (1972) in their studies of the roughness change problem and Neumann & Mahrer (1971) in a study of sea-breeze circulations. In these cases dynamic pressure effects were secondary; in the situation to be considered here they will be of primary importance.

* Received in original form 1975 April 21

## 2. The flow considered

In the long term we are interested in developing techniques for the study of three-dimensional boundary-layer flows above arbitrary topography. The problem considered here will however be an idealized two-dimensional situation and we will only consider the case of steady mean flow. In view of our three-dimensional aspirations we choose to work in terms of velocity and pressure rather than vorticity and stream function but we do allow ourselves the luxury of using conformal mappings to transform the flow region to a rectangle.

Consider the flow over a rigid rough wavy surface, periodic in $x$ with wavelength $L$ and with uniform surface roughness $z_0$. We assume the flow to be periodic in $x$ and to be driven by a horizontal kinematic shear stress, ${u_0}^2$ applied well above the region containing periodic flow variations caused by the surface topography (at a height $H \simeq 2{\cdot}5\,L$ is found to suffice). The situation is illustrated in Fig. 1 with a particular form for the lower boundary. In order to apply finite difference methods it is helpful if the boundaries of the flow region coincide with the co-ordinate mesh. This is achieved by a conformal mapping from cartesian co-ordinates $(x, y)$ to co-ordinates $(\xi, \eta)$

$$z = z(\zeta^*)$$

where $z = x + iy$ and $\zeta^* = \xi + i\eta$. As a simple example for which the lower boundary, $\eta = 0$, corresponds to an almost sinusoidal surface we take

$$z = \zeta^* + ia \exp(ik\zeta^*). \tag{1}$$

This is slightly different from that used by Benjamin (1959) (namely, $\zeta^* = z - iae^{ikz}$) in his treatment of flow over a wavy boundary and has the advantage that the Jacobian of the transformation

$$J = \frac{\partial(\xi, \eta)}{\partial(x, y)} = \left|\frac{dz}{d\zeta^*}\right|^{-2} \tag{2}$$

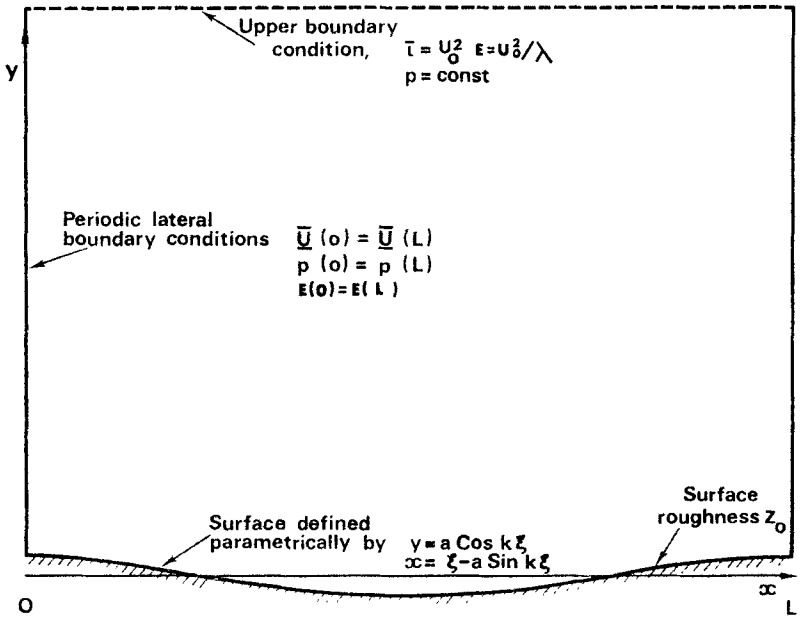


FIG. 1. Flow region with $ak = 0{\cdot}157$

may be computed directly at grid nodes in the $(\xi, \eta)$ plane. The surface $(\eta = 0)$ is given, parametrically, by

$$\left.\begin{aligned} y_b &= a\cos k\xi \\ x &= \xi - a\sin k\xi \end{aligned}\right\} \tag{3}$$

where $k = 2\pi/L$, and, for small amplitude, $a$, is approximately a simple cosine wave. However as $a$ increases the crests become shorter and steeper. (With Benjamin's transformation the troughs are sharper and the crests smoothed.)

Flow over surfaces of essentially this shape have been studied in the context of wind-wave generation. Recently Townsend (1972) and Long (1971) have used closure methods based on the turbulent energy equation in their solutions but both have linearized the problem in terms of the wave slope—a procedure which Townsend suspects when the wave slope $(ak)$ is $>0.1$. The numerical method developed in the present study is fully non-linear and can go beyond this range but, unfortunately, is inherently unstable if horizontal velocities become negative. Thus only the case of a fixed wave can be considered. This is of somewhat limited interest for wind-wave studies but is relevant for the study of the flow of water above sand or gravel waves.

We have chosen to drive the flow by an applied shear stress rather than specify a given velocity at the top of the model or to impose a given hydrostatic pressure gradient throughout the region. This offers considerable simplification in the formulation of the problem and helps to isolate the effect of the topography in modifying stress distributions and in perturbing the velocity profiles from their natural logarithmic form. It does however require that the boundary-layer is deep compared with $L$. If this is the case the friction velocity is the relevant velocity scale. Were we to impose a given current at a specified distance from the bed as our top boundary condition the results would be identical except for a constant scale factor. Clearly the situation in the field is far more complex than that considered here in that sand or gravel wave trains are rarely perfectly regular or of the precise shape considered, and more importantly, their wave length is frequently of a similar magnitude, and often related to the water depth. Extension of the model to allow for finite water depth and the presence of a free surface is a possible development of our model which we hope to investigate in the near future.

## 3. Equations and hypotheses

The equations of motion for steady, two-dimensional laminar flow of an inviscid, incompressible fluid in the transformed $(\xi, \eta)$ co-ordinate system may be written, for any conformal mapping, in the form

$$U\frac{\partial U}{\partial \xi} + V\frac{\partial U}{\partial \eta} - \frac{1}{2J}(J_\eta UV - J_\xi V^2) = -\frac{\partial p}{\partial \xi} \tag{4}$$

$$U\frac{\partial V}{\partial \xi} + V\frac{\partial V}{\partial \eta} - \frac{1}{2J}(J_\xi UV - J_\eta U^2) = -\frac{\partial p}{\partial \eta} \tag{5}$$

$$\frac{\partial}{\partial \xi}(J^{-\frac{1}{2}}U) + \frac{\partial}{\partial \eta}(J^{-\frac{1}{2}}V) = 0. \tag{6}$$

Here $U$ and $V$ are velocity components in the $\xi$ and $\eta$ directions respectively. While molecular viscosity will be unimportant in the momentum equations for the flows we are considering we must take account of turbulent stresses. These we may introduce, as in the cartesian co-ordinate case, by replacing $U$ by $\overline{U}+u'$, $V$ by $\overline{V}+v'$, $p$ by $\bar{p}+p'$, introducing additional $w'$ terms in the equations above and then ensemble averaging.

Combining $[\overline{(4)}+J^{\frac{1}{2}}\overline{u'(6)'}]$ (i.e. adding the mean of $J^{\frac{1}{2}}u'X$ the fluctuating part of equation (6) to the mean of equation (4)) we obtain:

$$\overline{U}\frac{\partial \overline{U}}{\partial \xi}+\overline{V}\frac{\partial \overline{U}}{\partial \eta}-\frac{1}{2J}(J_\eta \overline{U}\overline{V}-J_\xi \overline{V}^2)=-\frac{\partial \overline{p^*}}{\partial \xi}-\frac{\partial}{\partial \xi}\overline{(u'^2-v'^2)}-\frac{\partial}{\partial \eta}\overline{(u'v')}$$

$$+\frac{1}{2J}(J_\xi \overline{(u'^2-v'^2)}+2J_\eta \overline{u'v'}) \qquad (7)$$

while $[\overline{(5)}+J^{\frac{1}{2}}\overline{v'(6)'}]$ gives

$$\overline{U}\frac{\partial \overline{V}}{\partial \xi}+\overline{V}\frac{\partial \overline{V}}{\partial \eta}-\frac{1}{2J}(J_\xi \overline{U}\overline{V}-J_\eta \overline{U}^2)=-\frac{\partial \overline{p^*}}{\partial \eta}-\frac{\partial}{\partial \xi}\overline{(u'v')}$$

$$+\frac{1}{2J}(J_\eta \overline{(v'^2-u'^2)}+2J_\xi \overline{u'v'}). \qquad (8)$$

It is convenient to follow Townsend (1972) and set $\overline{p^*}=\bar{p}+\overline{v'^2}$. We will subsequently drop the * and refer to $\overline{p^*}$ as pressure in what follows. The mean continuity equation takes the form

$$\frac{\partial}{\partial \xi}(J^{-\frac{1}{2}}\overline{U})+\frac{\partial}{\partial \eta}(J^{-\frac{1}{2}}\overline{V})=0. \qquad (9)$$

We are now faced with the usual closure problem for turbulent flow. In the development of the models to be described a sequence of alternative hypotheses were made. In general the results were not unduly sensitive to the detailed assumptions made with the exception of differences between mixing-length (ML) models and those incorporating the turbulent energy equation (TE models). We will concentrate on the description of a particular basic TE model but will also give some results from a ML model and a model using the scalar eddy viscosity suggested by Hinze (1959).

The stress–strain closure assumption used within the basic TE model is that

$$\tau = l(\lambda \bar{E})^{\frac{1}{2}}\frac{\partial}{\partial \eta}(J^{\frac{1}{2}}\overline{U}) \qquad (10)$$

where $\tau=-\overline{u'v'}$, $\bar{E}=\frac{1}{2}(\overline{u}'^2+\overline{v}'^2+\overline{w}'^2)$ and $\lambda$ is a constant, equal to the equilibrium value of the ratio $u_0{}^2/\bar{E}$. A value of 0·25 is used here based on current estimates for the surface boundary layer of the atmosphere (see Monin & Yaglom (1971, p. 517–520) and Busch (1973)). The length scale, $l$, for the mixing process is a prescribed function of position. This approach was preferred to setting $\tau \propto \bar{E}$.

In effect equation (10) assumes that the flow is essentially parallel to the lines $\eta=$ const in that it neglects the rate of strain $(\partial/\partial\xi)(J^{\frac{1}{2}}\overline{V})$ from the expression that would hold with a scalar eddy viscosity, namely

$$\tau = l(\lambda \bar{E})^{\frac{1}{2}}\left\{\frac{\partial}{\partial \xi}(J^{\frac{1}{2}}\overline{V})+\frac{\partial}{\partial \eta}(J^{\frac{1}{2}}\overline{U})\right\}. \qquad (10a)$$

Equation (10) can be thought of as containing a plane shear term $J^{\frac{1}{2}}(\partial\overline{U}/\partial\eta)$ and a curvature term $\overline{U}(\partial J^{\frac{1}{2}}/\partial\eta)$. In the flow situations considered here the effect of the $(\partial/\partial\xi)$ term would often be to reduce the contribution from the curvature term. This is simply stating that the flow will be less curved than the co-ordinate system, which corresponds to the streamlines for ideal flow.

In most of the region the plane shear term $J^{\frac{1}{2}}(\partial\overline{U}/\partial\eta)$ will dominate, especially near the surface. However, there will be a region of reduced shear a little above the crest where, as the amplitude of the surface waviness increases, we may find that the other terms are important.

The choice of $l$ is not unambiguous and after trials with $l \propto (\eta + z_0)$ and with

$$l \propto \int_0^{\eta} ds + z_0$$

(the integral being taken along lines $\xi$ = const.) the final form adopted was

$$l = \kappa(\eta + z_0)\,(1 - \mathrm{e}^{-k\eta}) + \kappa(s + z_0)\,\mathrm{e}^{-k\eta} \tag{11}$$

where

$$s = \int_0^{\eta} J^{-\frac{1}{2}}\,d\eta,$$

$z_0$ is the surface roughness length and $\kappa$ is von Karman's constant (0·4). Thus near the lower boundary $l \propto (s + z_0)$, $s$ being the local distance from the wall while at large distances $l \propto \eta$, an average distance from the wall. This is essentially the same form as that adopted by Townsend (1972) for his dissipation length. Provided $l \simeq \kappa(s + z_0)$ near the wall, which is well established, the results will be relatively insensitive to other details.

We also assume a fixed partitioning of the turbulent energy with

$$\overline{u'^2} = 1{\cdot}0\bar{E};\ \overline{v'^2} = 0{\cdot}35\bar{E};\ \overline{w'^2} = 0{\cdot}65\bar{E}. \tag{12}$$

In the absence of accepted values for marine boundary-layers the constants are again based on Monin & Yaglom's (1971) and Busch's (1973) atmospheric data. We would anticipate similar values in the sea and can also remark that the model predictions are not at all sensitive to this partitioning of $\bar{E}$. Note that $y$ is the vertical direction in the notation used here. In the ML model we assume

$$\overline{u'^2} - \overline{v'^2} = 2{\cdot}6\,u_0^2 \text{ (constant)}$$

which is equivalent to the assumption in equations (12) if $u_0^2 \equiv 0{\cdot}25\,E$, and

$$\tau^{\frac{1}{2}} = l\frac{\partial}{\partial\eta}(J^{\frac{1}{2}}\,\overline{U}).$$

The turbulent energy equation in $(\xi, \eta)$ co-ordinates may be obtained by analogy with the standard procedure for cartesian co-ordinates and can be written, including the time rate of change for reference, as

$$\begin{aligned} J^{-\frac{1}{2}}\frac{\partial\bar{E}}{\partial t} + \overline{U}\frac{\partial\bar{E}}{\partial\xi} + \overline{V}\frac{\partial\bar{E}}{\partial\eta} - \frac{J_\eta}{2J}(\overline{u'^2}\,\overline{V} + \tau\overline{U}) - \frac{J_\xi}{2J}(\overline{v'^2}\,\overline{U} + \tau\overline{V}) \\ = \tau\left[\frac{\partial\overline{U}}{\partial\eta} + \frac{\partial\overline{V}}{\partial\xi}\right] - \overline{u'^2}\frac{\partial\overline{U}}{\partial\xi} - \overline{v'^2}\frac{\partial\overline{V}}{\partial\eta} - J^{\frac{1}{2}}\frac{\partial}{\partial\xi}[J^{-\frac{1}{2}}(\overline{u'p'} + \overline{u'E'})] \\ - J^{\frac{1}{2}}\frac{\partial}{\partial\eta}[J^{-\frac{1}{2}}(\overline{v'p'} + \overline{v'E'})] - J^{-\frac{1}{2}}\varepsilon \end{aligned} \tag{13}$$

where $\varepsilon$ is the rate of viscous dissipation of turbulent energy.

The additional closure hypotheses used within the turbulent energy equation are

$$\left.\begin{aligned} &\overline{v'p'}+\overline{v'E'} = -J^{\frac{1}{2}}K_E\frac{\partial \bar{E}}{\partial \eta}; \quad K_E = l(\lambda \bar{E})^{\frac{1}{2}} \\ &\varepsilon = (\lambda \bar{E})^{\frac{3}{2}}/l_D; \quad l_D \text{ is taken equal to } l \end{aligned}\right\} \tag{14}$$

Horizontal diffusion of turbulent energy is not included explicitly and $\overline{u'p'}+\overline{u'E'}$ is neglected. There is, however, a small amount of residual horizontal diffusion associated with the finite difference scheme (see Appendix). The hypotheses used here are analogous to closure assumptions frequently made at this level in cartesian co-ordinates (e.g. Taylor 1973).

Boundary conditions to be imposed on the solution are

$$\left.\begin{aligned} &\text{on} \quad \eta = 0 : \bar{U} = \bar{V} = 0, \quad \frac{\partial \bar{E}}{\partial \eta} = 0 \\ &\text{on} \quad \eta = H : \tau = u_0^2, \quad \bar{p} = 0 \quad \text{and} \quad \bar{E} = u_0^2/\lambda. \end{aligned}\right\} \tag{15}$$

We anticipate (correctly) that the results will show $\bar{V} \simeq 0$ at the upper boundary. This serves as one check on the validity of the numerical solutions obtained.

The lateral boundary conditions are of periodicity $L$ in $\xi$ so that

$$\bar{U}(0) = \bar{U}(L), \; \bar{V}(0) = \bar{V}(L), \; \bar{E}(0) = E(L) \text{ and } \bar{p}(0) = \bar{p}(L).$$

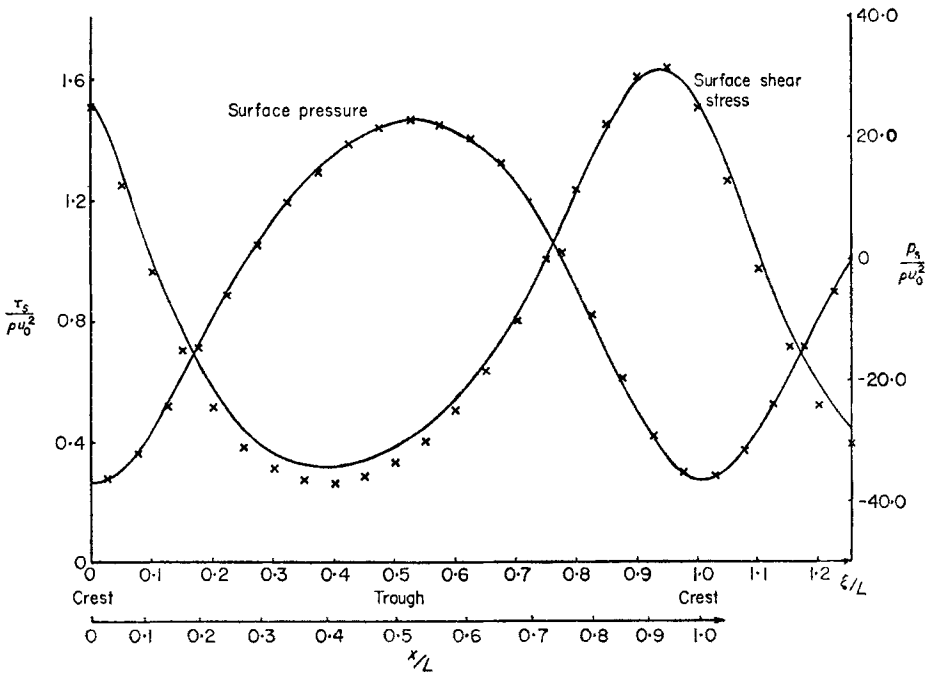


FIG. 2. Surface shear stress and pressure plotted against $\xi/L$ and $x/L$. $L/z_0 =$ 10 000; $ak = 0{\cdot}157$; —— Turbulent energy equation model; $X$ Mixing-length model.

In most turbulent boundary layers the logarithm of the distance from the wall is the relevant 'vertical' co-ordinate and we acknowledge this by making the transformation

$$\zeta = \ln\left(\frac{\eta + z_0}{z_0}\right). \tag{16}$$

We also scale velocities wrt $u_0$ and lengths wrt $z_0$ to give a non-dimensional set of equations prior to attempting their numerical solution. The numerical methods used are described in the Appendix.

## 4. Results for a typical case

The initial application of this work is intended to be in the study of the flow of water above sand and gravel waves. A gravel wave in the Solent area (between the mainland and the Isle of Wight in Southern England) can be approximately sinusoidal with a wavelength of 10 m and an amplitude of 0·25 m (Dyer 1970). If we take the roughness length to be 0·1 cm then we have $L/z_0 = 10\,000$ and $a/z_0 = 250$ in our idealized model. The approximate maximum wave slope, $ak$, will be 0·157 as in Fig. 1.

We have obtained results for this case using both our mixing-length and turbulent energy equation models. Predictions of surface shear stress, $\tau_s$, and surface pressures $(\bar{p}+\overline{v'^2})_s$ are given in Fig. 2. The ML model precits slightly larger amplitude variations in surface shear stress than the TE model while the pressure fields are essentially the same for the two models. Phase differences (in $\xi$) of the maxima relative to the waveform are about the same in both cases ($-22°$ for the stresses and $+191°$ for the pressures). Velocity profiles are also quite similar as can be seen in Fig. 3, which shows velocity profiles $\bar{U}(\eta)$ at a series of positions on the wave. It should be remarked that these are velocities parallel to the lines $\eta$ = constant and are plotted at fixed values of $\xi$ rather than in the original rectangular co-ordinates. They do show considerable variations from the logarithmic form and are not unlike some of the profiles given by Dyer (1970, Fig. 2). In Fig. 4 we show contours for the pressure field in the $(\xi, \zeta)$ plane. It is immediately apparent that the phase of the pressure disturbance changes very little with distance from the wall. Pressure extrema occur only at the surface and, as can also be seen in Fig. 2 the negative extremum is con-

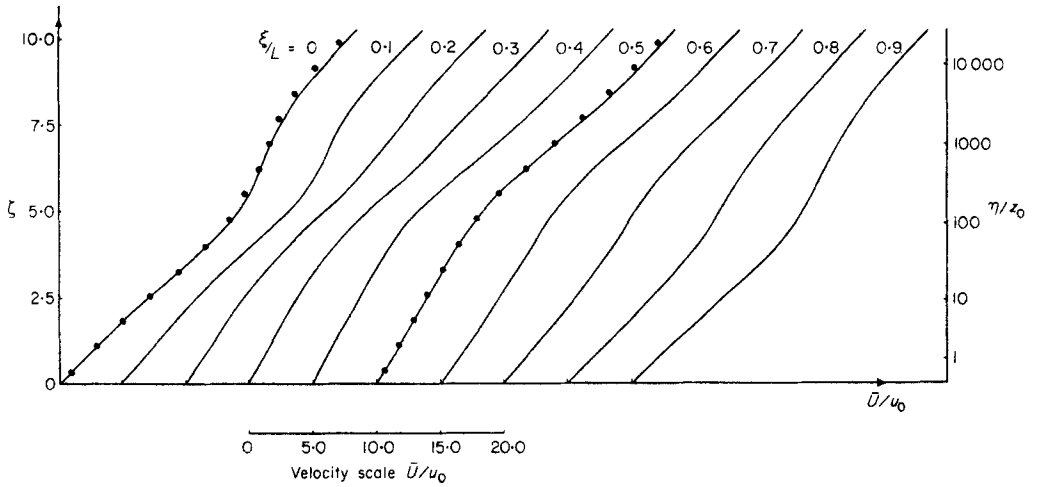


FIG. 3. Velocity profiles; $L/z_0 = 10\,000$; $ak = 0·157$; ——Turbulent energy equation model; • Mixing-length model.

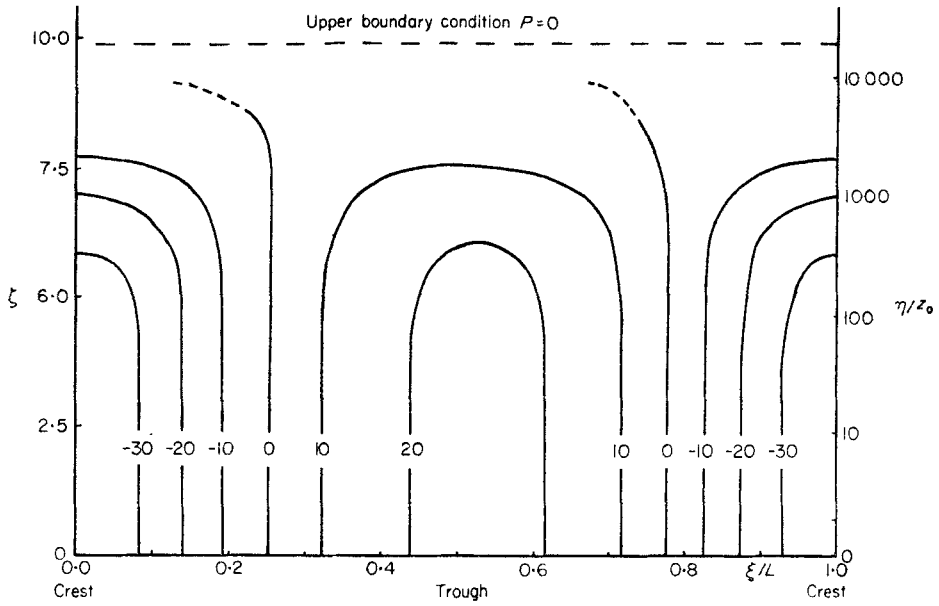


FIG. 4. Pressure field; $L/z_0 = 10\,000$; $ak = 0{\cdot}157$ (TE model).

siderably larger in magnitude than the positive one. When the net vertical stress on the lower boundary is computed however it is approximately zero and an overall stress balance for the integration region is obtained to within about 1 per cent of the applied shear stress. While the phase of the surface pressure distribution relative to the surface is only slightly different from 180° this asymmetry does give rise to a

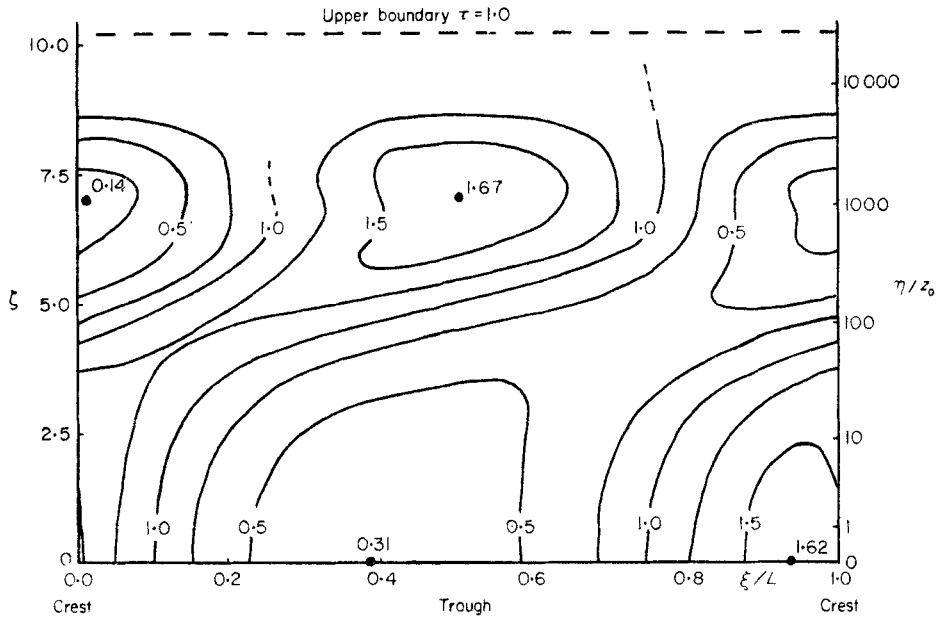


FIG. 5. Shear stress contours; $L/z_0 = 10\,000$; $ak = 0{\cdot}157$ (TE model).

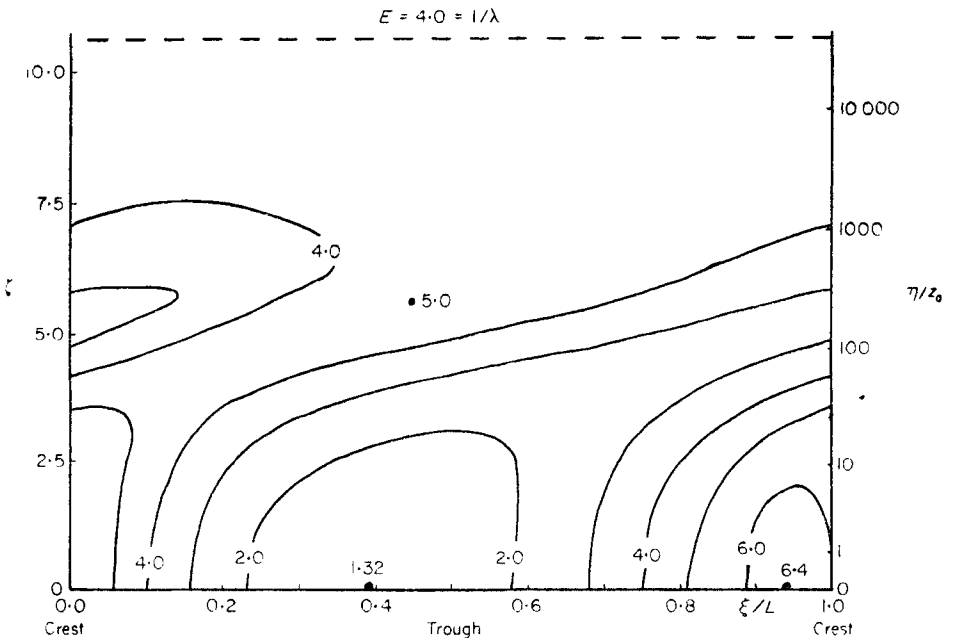


FIG. 6. Turbulent energy contours; $L/z_0 = 10\,000$; $ak = 0{\cdot}157$.

contribution to the mean horizontal stress on the lower boundary, $0{\cdot}22\,u_0^2$ in this case. ($0{\cdot}26\,u_0^2$ with the mixing length model). The horizontal contribution of the shear stress at the surface is correspondingly reduced to $0{\cdot}78\,u_0^2$ ($0{\cdot}74\,u_0^2$).

The distributions of shear stress and turbulent energy are shown in Figs 5 and 6. There are considerable variations in the phase and the amplitude of the perturbation in shear stress (from its average value for a given $\eta$) with distance from the lower boundary. At the surface there is a stress maximum a little way upstream of the crest and a minimum upstream of the trough. There are however additional extrema about 180° out of phase with these at a height of about $0{\cdot}1\,L$ above the surface. These figures are plotted with a logarithmic scale in $\eta$ and the fluid volume or depth associated with these elevated extrema is considerably (about 100 times) larger than for the surface features. It is not unreasonable to expect therefore that the most pronounced features of vertical profiles of turbulent shear stress, or to a lesser extent turbulent energy, would be maxima above the trough and minima above the crest.

## 5. Effects of variation in amplitude and roughness

A series of computations have been made keeping $L/z_0$ fixed at 10 000 and varying $a/z_0$. We have only been able to obtain stable results with $a/z_0 \leqslant 400$. From these results we estimate that mean flow separation would occur with $a/z_0 \simeq 500$ ($ak = 0{\cdot}314$). Fig. 7 shows the computed maximum and minimum shear stresses. Variations with $a/z_0$ are approximately linear over the lower part of the range shown. The values for these maxima and their phases are also given in Table 1. The changes in phase with amplitude may be partly due to the changes in shape of the wave. Note that as the amplitude of the wave increases so the proportion of the horizontal force on the lower boundary due to horizontal shear surface stress, $\langle \tau_{surf} \rangle$ decreases. This is compensated for by an increase in the horizontal component of the surface pressure forces arising partly from an increase in magnitude and partly from a change of phase angle.

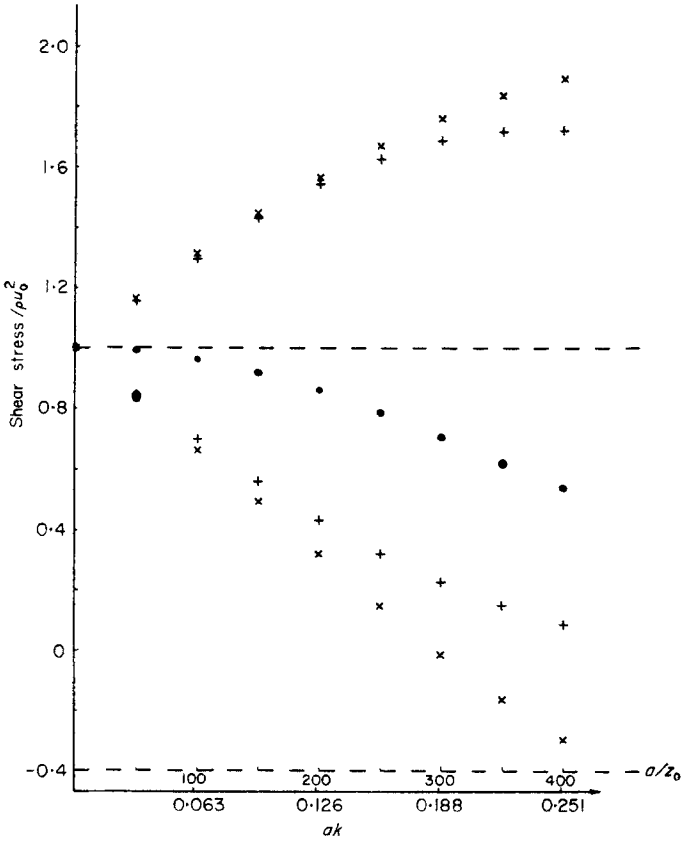


FIG. 7. Variation of shear stress values with wave amplitude; $L/z_0 = 10\,000$. +, surface extreme values; $X$, elevated extrema; •, average horizontal component of surface shear stress.

In order to investigate the effect of surface roughness a series of computations for different values of $L/z_0$ were made with $ak$ fixed at 0·157. Some of the results are given in Table 2. Perhaps the most notable feature of these results is that as the roughness length is decreased the range of the variations in surface shear stress decreases but the elevated shear stress extrema become more pronounced. For the smoother surfaces the elevated extrema become absolute extrema in the sense that overall maximum and minimum shear stresses no longer occur at the surface. These elevated extrema occur at a height which is virtually independent of roughness length, at $\eta/L \simeq 0{\cdot}1$. As we may expect the contribution of the pressure field to the average horizontal stress increases with decreasing roughness as may be seen from the values for $\langle \tau_{surf} \rangle$. The increase in magnitude of the pressures, scaled wrt $u_0^2$, as the roughness decreases reflects the decrease in $u_0$ under these circumstances.

## 6. Some effects of variation in shape

We have noted in Section 2 that the surface configuration (3) corresponding to the transformation (1) is not identical to a cosine wave, nor is that corresponding to Benjamin's (1959) transformation for which

$$y_b(x) = ae^{-ky_b} \cos kx. \tag{17}$$

**Table 1**

*Effects of wave amplitude variation;* $(L/z_0) = 10\,000$

| | | | Surface shear stress | | | Elevated stress extrema | | Surface pressure field | | |
|---|---|---|---|---|---|---|---|---|---|---|
| | | | | | Phase of* | | | | | Phase of* |
| $a/z_0$ | $ak$ | $\langle\tau_{surf}\rangle$ | $\tau_{max}$ | $\tau_{min}$ | $\tau_{max}$ | $\tau_{max}$ | $\tau_{min}$ | $p_{max}$ | $p_{min}$ | $p_{max}$ |
| 0 | 0 | 1·0 | 1·0 | 1·0 | — | 1·0 | 1·0 | 0·0 | 0·0 | — |
| 50 | 0·031 | 0·99 | 1·15 | 0·85 | (a) −28° | 1·16 | 0·83 | 6·8 | −7·4 | (a) 186° |
| | | | | | (b) −27° | | | | | (b) 186° |
| 100 | 0·063 | 0·96 | 1·29 | 0·70 | (a) −26° | 1·31 | 0·66 | 12·6 | −14·8 | (a) 187° |
| | | | | | (b) −25° | | | | | (b) 187° |
| 150 | 0·094 | 0·92 | 1·42 | 0·56 | (a) −25° | 1·44 | 0·49 | 17·3 | −22·8 | (a) 188° |
| | | | | | (b) −22° | | | | | (b) 189° |
| 200 | 0·126 | 0·86 | 1·54 | 0·43 | (a) −23° | 1·56 | 0·31 | 20·6 | −30·0 | (a) 190° |
| | | | | | (b) −21° | | | | | (b) 191° |
| 250 | 0·157 | 0·78 | 1·62 | 0·32 | (a) −22° | 1·67 | 0·14 | 22·7 | −36·1 | (a) 191° |
| | | | | | (b) −19° | | | | | (b) 193° |
| 300 | 0·188 | 0·71 | 1·69 | 0·22 | (a) −21° | 1·76 | −0·02 | 23·6 | −41·4 | (a) 193° |
| | | | | | (b) −17° | | | | | (b) 196° |
| 350 | 0·220 | 0·62 | 1·72 | 0·15 | (a) −20° | 1·83 | −0·16 | 23·4 | −45·2 | (a) 196° |
| | | | | | (b) −16° | | | | | (b) 199° |
| 400 | 0·251 | 0·54 | 1·72 | 0·08 | (a) −19° | 1·89 | −0·29 | 22·3 | −47·3 | (a) 199° |
| | | | | | (b) −14° | | | | | (b) 203° |

* Phase relative to crest of underlying surface wave, (a) based on $\xi$ value, (b) based on $x$ value. Stresses are scaled wrt $u_0^2$.

**Table 2**

*Effects of surface roughness variation*; $(a/L) = 0{\cdot}025$ $ak = 0{\cdot}157$

| | | | Surface shear stress | | | Elevated stress extrema | | Surface pressure field | | |
|---|---|---|---|---|---|---|---|---|---|---|
| | | | | | Phase of* | | | | | Phase of* |
| $L/z_0$ | $a/z_0$ | $\langle\tau_{surf}\rangle$ | $\tau_{max}$ | $\tau_{min}$ | $\tau_{max}$ | $\tau_{max}$ | $\tau_{min}$ | $p_{max}$ | $p_{min}$ | $p_{max}$ |
| †400 | 10 | 0·84 | 1·74 | 0·33 | −23° | 1·50 | 0·39 | 6·5 | −9·8 | 205° |
| 2 000 | 50 | 0·80 | 1·70 | 0·31 | −25° | 1·59 | 0·28 | 13·0 | −20·4 | 197° |
| 10 000 | 250 | 0·78 | 1·62 | 0·32 | −22° | 1·67 | 0·14 | 22·7 | −36·1 | 191° |
| 40 000 | 1 000 | 0·77 | 1·56 | 0·34 | −20° | 1·75 | −0·02 | 33·6 | −53·9 | 188° |

Stresses are sealed wrt $u_0{}^2$. * Phase relative to crest of underlying surface wave based on $\xi$ value. † 96 per cent correction for upstream differences (other cases have 97 per cent)—see Appendix for details.

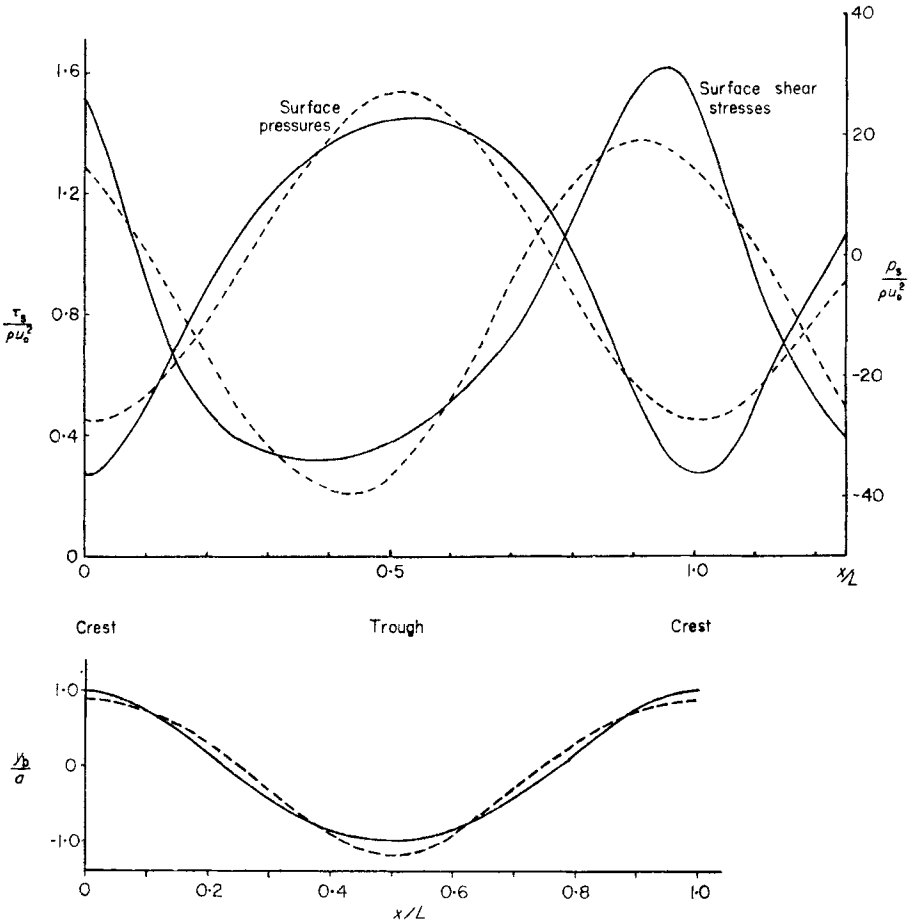


FIG. 8. Surface pressure and shear stresses plotted against $x/L$. ——, transformation (1); – – –, Brooke–Benjamin transformation $ak = 0{\cdot}157$ $L/z_0 = 10\,000$. The shapes of the underlying surface are also plotted.

In order to illustrate the effects of these differences computations have been made using the basic TE model with Benjamin's transformation for the case $ak = 0{\cdot}157$, $L/z_0 = 10\,000$. The resulting surface shear stress and pressure are shown in Fig. 8. The differences are quite pronounced and consistent with the notion that (17) gives rise to sharper troughs and smoother crests than equation (1). For Benjamin's transformation the elevated shear stress maximum, over the trough, is approximately $1{\cdot}90\,u_0^2$ while the minimum is $0{\cdot}31\,u_0^2$ compared with $1{\cdot}67\,u_0^2$ and $0{\cdot}14\,u_0^2$. Both occur, as before at $(\eta/L) \simeq 0{\cdot}1$ and $\langle\tau_{\text{surf}}\rangle$ is again $0{\cdot}78\,u_0^2$. The phase of the surface shear stress maximum is reduced in the Benjamin case to $-31°$ (in $x$) compared to $-19°$ while the phase of the minimum is advanced towards the trough. The pressure maximum remains in approximately the same place, $x = 191°$ for the Benjamin case compared to 193°. Both the surface shear stress and pressure distributions take on a somewhat more sinusoidal appearance than in the case with transformation (1).

The underlying surface can be made closer to a pure cosine wave by adding higher harmonics to the conformal mapping. If

$$z = \zeta^* + ia\left[\left(1 - \frac{3a^2k^2}{8}\right)e^{ik\zeta^*} + \frac{ak}{2}(1 - e^{2ik\zeta^*}) + \frac{3a^2k^2}{8}e^{3ik\zeta^*}\right] \qquad (18)$$

**Table 3**

*Stress extrema etc. with standard and cosine wave models*: $(L/z_0) = 10\,000$

| | | $a/z_0 = 250$ Standard | $ak = 0{\cdot}157$ Cosine wave | $a/z_0 = 350$ Standard | $ak = 0{\cdot}22$ Cosine wave |
|---|---|---|---|---|---|
| $\langle\tau_{surf}\rangle$ | | 0·78 | 0·79 | 0·62 | 0·64 |
| Surface shear stress | $\tau_{max}$ | 1·62 | 1·48 | 1·72 | 1·47 |
| | $\tau_{min}$ | 0·32 | 0·28 | 0·15 | 0·11 |
| | $\varepsilon^*$ | −19° | −23° | −16° | −22° |
| Elevated shear stress | $\tau_{max}$ | 1·67 | 1·74 | 1·83 | 1·98 |
| | $\tau_{min}$ | 0·14 | 0·24 | −0·16 | 0·02 |
| Surface Pressure field | $p_{max}$ | 22·7 | 24·8 | 23·4 | 26·5 |
| | $p_{min}$ | −36·1 | −31·1 | −45·2 | −36·6 |
| | $\varepsilon^*$ | 193° | 192° | 199° | 196° |

* $\varepsilon$ are phases in $x$ relative to the crest of the underlying wave

the surface is given by

$$y = a\cos kx + 0(a^4 k^3).$$

Several runs were made for $(L/z_0) = 10\,000$ with this profile in the basic model and then compared to the previous results. For $a = 50z_0$, the differences were very small being less than 1 per cent in all the variables. For higher amplitudes the differences became more pronounced, and a comparison is shown in Table 3.

Pressure showed slight differences in that the range was decreased for the cosine wave and the distribution became less asymmetric (about $p = 0$). The phase reduced fractionally and the contribution to the surface stress due to form drag was slightly reduced. The surface shear stress maximum is reduced and moved further back from the wave crest for the cosine wave case. The reduced surface shear stress minima indicate that mean flow separation is now predicted for a smaller amplitude than for the standard model.

In all cases considered in this section the overall picture of the flow field remains essentially the same as that described in Section 4 but it may be noted that the changes in shape do give rise to changes in surface shear stress which may be significant if we are concerned with the sediment transport over such bed forms.

## 7. Comparisons with other studies

As noted in Section 2 there have been several previous studies, both theoretical and experimental, on flow above wavy surfaces. The main application lies in the field of wind-wave generation and the case of a rigid lower boundary is often treated only briefly as a special case. We first discuss some comparisons with recent experimental work. As noted by Ursell (1956) the experiments conducted by Motzfeld (1937) are somewhat unsatisfactory in that he only used three sinusoidal waves to generate the flow which would not have reached a ' fully developed ' state. This factor does not appear to be as important in recent wind-tunnel work by Kendall (1970) where 12 waves are used. His boundary-layer thickness is however still only about $0{\cdot}75\,L$. Comparisons with the present work are also hindered by the fact that his experiment was made with a smooth wall. We will concentrate our attention on his case with the free stream velocity, $u_\infty = 5{\cdot}5\,\mathrm{ms}^{-1}$. His experiment had $L = 10{\cdot}16\,\mathrm{cm}$ and $a = 0{\cdot}317\,\mathrm{cm}$ which give $ak = 0{\cdot}196$. We also used Kendall's values of $kz_0 = 0{\cdot}0016$ which gives $z_0 = 0{\cdot}0026\,\mathrm{cm}$ and $u_0 = 0{\cdot}4\times 0{\cdot}118\,u_\infty$ corresponding to $u_0 \simeq 26\,\mathrm{cm\,s}^{-1}$. Here $u_0$ is an average surface friction velocity, and appears to be based on an average velocity profile over the wave form. If the flow were hydraulically

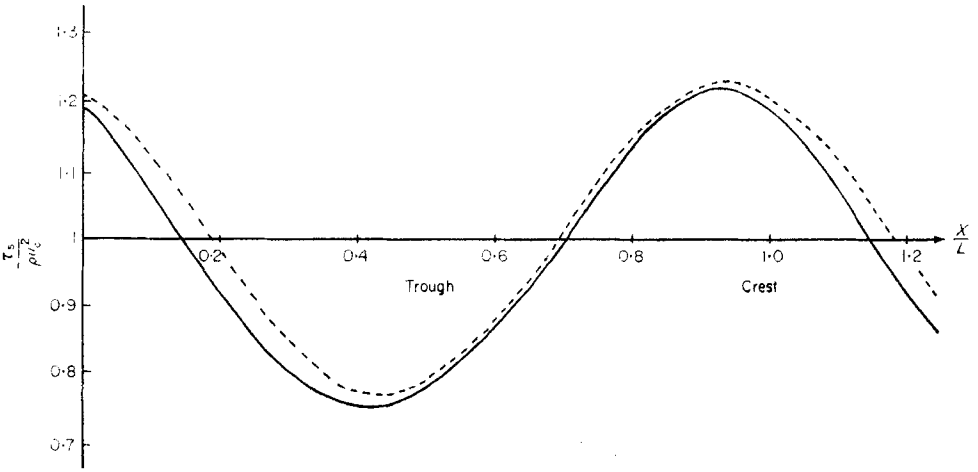


FIG. 9. Surface shear stress against $x/L$. $kz_0 = \exp(-8)$ $ak = 0{\cdot}05$; ——, turbulent energy equation model; – – –, Townsend's linear theory.

smooth the effective $z_0$ could vary by a factor 2.7 with position along the wave. In Kendall's case the flow is probably transitional between hydraulically smooth and rough as taking $\nu(\text{air}) = 0{\cdot}14\,\text{cm}^2\,\text{s}^{-1}$ gives an effective $z_0$ $(= \nu/9u_0)$ of 0·0006 cm. This is not much smaller than the value assumed above. Also the fact that $\langle\tau_{\text{surf}}\rangle \neq \langle u_0\rangle^2$, means that the above value of $u_0$ may be an underestimate since the pressure forces provide a third of the total drag on the surface according to Kendall's results.

In spite of these problems we have run our model for constant $z_0$ with $ak = 0{\cdot}196$ and $L/z_0 = 3928$. We have used the cosine wave transformation equation (18).

Consider first the wall shear stress measurements, Fig. 15 of Kendall's paper. We note that the phases are different ($-70°$ from Kendall's experiment and about $-22°$ (in $x$) for the present results) and there are considerable differences in the shapes of the curves with the experimental results showing almost a sawtooth pattern in contrast to the model prediction of a relatively smooth shear stress minimum similar to that shown in Fig. 10. There is a tendency to increased asymmetry in our surface shear stress results with increasing wave amplitude but no indication of such a sharp minimum. Kendall's wall stress meter was not calibrated but gave a ratio of maximum to minimum surface shear stresses of 7·5. Our computations give 10.

Surface pressure results are given by Kendall in his Fig. 3. Our computed results give values of $(p_{\max}-p_{\min})/\rho u_0{}^2$ of 45·2. The values given by Kendall's Fig. 3 with $u_0/u_\infty = 0{\cdot}0472$ give $(p_{\max}-p_{\min})/\rho u_0{}^2 = 44{\cdot}9$. There is also agreement in the phase for which Kendall gives a value of 195·6° for the fundamental wave number on a harmonic analysis while we have 197° based on the location of the maximum. Kendall also shows an increase of this phase angle with roughness (decreasing Reynolds number) in agreement with Table 2. Kendall computes pressure drag assuming a simple sinusoidal surface pressure field and gives values from which we find a ratio of pressure drag to total surface drag of 33 per cent. This is slightly higher than the model prediction of 28·7 per cent but the agreement is encouraging.

The mean velocity field results shown by Kendall (Fig. 6 of this paper) agree in some qualitative features with our computations. The perturbation from the mean, essentially logarithmic profile has a maximum at about $y/L = 0{\cdot}01 \sim 0{\cdot}02$ and extends to $y/L = 0{\cdot}25$. The maximum range of his perturbation may be estimated as $8{\cdot}3\,u_0$ from Kendall's paper which is somewhat larger than our computed value of about $5{\cdot}8\,u_0$.

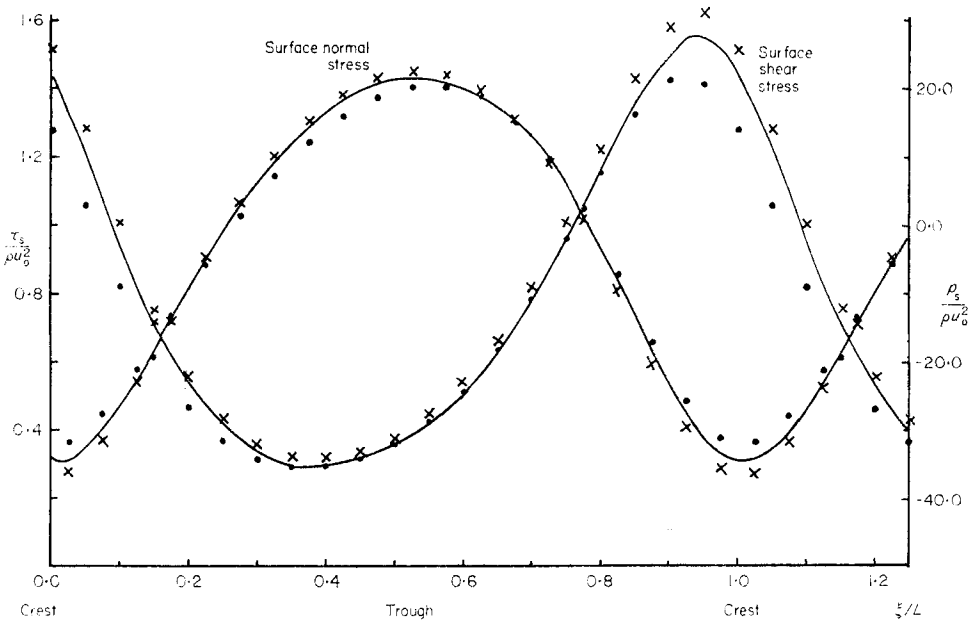


FIG. 10. Differences in surface stresses between standard and 'Isotropic eddy viscosity' models. $L/z_0 = 10\,000$; $ak = 0{\cdot}157$; $X$, standard model; ——, isotropic eddy viscosity model; ●, isotropic model with curvature modifications, $\alpha = 5{\cdot}0$.

All things considered there seems quite fair agreement between the model predictions and Kendall's measurements except in the form of the variation of wall shear stress. At present we are unable to account for this but we can note that Kendall's shear stress results are not substantiated by the observations of Hsu & Kennedy (1971). Their experiments were carried out in a tube with a sinusoidal longitudinal section. Although the wavelength of the sine waves is greater than the diameter of the tube, comparison between their results taken at the wall of the tube and our lower surface values is possibly relevant. Hsu and Kennedy give results for two runs with $a/L$ equal to 1/45 (Case I) and 1/90 (Case II). Their Fig. 5 shows wall pressures that are closer to sine waves than are our predictions but there is agreement in the location of the pressure minimum, slightly downstream from the wave crest. (The location of the maximum is difficult to determine from their figure.) Their Fig. 9 gives wall shear stress profiles which again show a very sinusoidal pattern. They give values for the location of the shear stress maximum of $-26°$ for $a/L = 1/45$ and $-18°$ for $a/L = 1/90$ compared to the wave crest. Results for our cosine wave case give $-23°$ for $a/L = 1/40$.

As a comparison of the magnitude of shear stress variation we note that the ratio $(\tau_{max}-\tau_{min})/\frac{1}{2}(\tau_{max}+\tau_{min})$ has a value of 1·28 for Hsu & Kennedy's model I and 1·07 for model II. For our cosine model with $a/L = 1/40$ we have a value of 1·36 which is in reasonable agreement. More detailed comparison is not justified as there are considerable differences between our model and these experiments. The use of smooth walls and the consequent importance of the viscous shear layer near the wall is perhaps the most serious of these.

On the theoretical side perhaps the most appropriate comparison to make is with Townsend's (1972) recent linear theory. The turbulent energy equation is included in his model with similar closure assumptions to those used here. The case of interest (i.e. with $c = 0$) for which results are given by Townsend is for $R = -\ln(kz_0) = 8$.

The surface stresses are compared in Fig. 9, where we have taken $ak = 0{\cdot}05$ in the cosine wave model and scaled quantities wrt $\tau_0 = {u_0}^2$. Setting $\tau_0 = \langle \tau_{\text{surf}} \rangle$ would produce only slight changes, but would bring the curves in Fig. 9 closer together. The general agreement is very good, the slight phase differences in the stress field probably being attributable to the different shear stress hypotheses in the two studies.

## 8. Isotropic eddy viscosity model

So far the stress-strain relation assumed, equation (10), has relied for its validity on the flow being approximately parallel to the lines $\eta =$ constant. If we simply replace (10) by (10a) we find that our numerical scheme fails and that in order to retain numerical stability we must also express the $\overline{u'^2}$ and $\overline{v'^2}$ Reynolds stresses appearing in the momentum equation in terms of mean flow derivatives. A consistent approach to this is suggested by Hinze (1959, p. 21) which, in our curvilinear co-ordinate scheme, gives

$$\left.\begin{aligned} -\overline{u'^2}+\tfrac{2}{3}\bar{E} &= (\lambda\bar{E})^{\frac{1}{2}}\, l\left\{\frac{\partial}{\partial\xi}(J^{\frac{1}{2}}\bar{U})-\frac{\partial}{\partial\eta}(J^{\frac{1}{2}}\bar{V})\right\} \\ -\overline{v'^2}+\tfrac{2}{3}\bar{E} &= (\lambda\bar{E})^{\frac{1}{2}}\, l\left\{\frac{\partial}{\partial\eta}(J^{\frac{1}{2}}\bar{V})-\frac{\partial}{\partial\xi}(J^{\frac{1}{2}}\bar{U})\right\} \\ -\overline{w'^2}+\tfrac{2}{3}\bar{E} &= 0 \end{aligned}\right\} \qquad (19)$$

in addition to equation (10a).

Summation of these equations leads to a null balance and they cannot be used to determine the value of $\bar{E}$. Clearly they could lead to anomalous negative values of $\bar{u}'^2$ or $\bar{v}'^2$ (in practice they have not) and are inconsistent with the partitioning of energy found in most boundary-layers (equation (12)). However, our model is fairly insensitive to this partitioning and this aspect of the modification to our model is not very significant.

For the present model we define as $\overline{p^{**}}$ by

$$\overline{p^{**}} = \bar{p} + \frac{2\bar{E}}{3}$$

and after some manipulation we can write the momentum equations in the form

$$\begin{aligned} &\bar{U}\frac{\partial\bar{U}}{\partial\xi}+\bar{V}\frac{\partial\bar{U}}{\partial\eta}-\frac{1}{2J}(J_\eta\bar{U}\bar{V}-J_\xi\bar{V}^2) \\ &\quad=-\overline{p_\xi^{**}}+K\left[\frac{\partial^2}{\partial\xi^2}(J^{\frac{1}{2}}\bar{U})+\frac{\partial^2}{\partial\eta^2}(J^{\frac{1}{2}}\bar{U})\right] \\ &\qquad+\left(K_\xi-\frac{KJ_\xi}{J}\right)\left[\frac{\partial}{\partial\xi}(J^{\frac{1}{2}}\bar{U})-\frac{\partial}{\partial\eta}(J^{\frac{1}{2}}\bar{V})\right] \\ &\qquad+\left(K_\eta-\frac{KJ_\eta}{J}\right)\left[\frac{\partial}{\partial\xi}(J^{\frac{1}{2}}\bar{V})+\frac{\partial}{\partial\eta}(J^{\frac{1}{2}}\bar{U})\right] \end{aligned} \qquad (20)$$

and

$$\overline{U}\frac{\partial \overline{V}}{\partial \xi}+\overline{V}\frac{\partial \overline{V}}{\partial \eta}-\frac{1}{2J}\left(J_\xi \overline{U}\overline{V}-J_\eta \overline{U}^2\right)$$

$$=-\overline{p_\eta}^{**}+K\left[\frac{\partial^2}{\partial \xi^2}\left(J^{\frac{1}{2}}\overline{V}\right)+\frac{\partial^2}{\partial \eta^2}\left(J^{\frac{1}{2}}\overline{V}\right)\right]$$

$$+\left(K_\eta-\frac{KJ_\eta}{J}\right)\left[\frac{\partial}{\partial \eta}\left(J^{\frac{1}{2}}\overline{V}\right)-\frac{\partial}{\partial \xi}\left(J^{\frac{1}{2}}\overline{U}\right)\right]$$

$$+\left(K_\xi-\frac{KJ_\xi}{J}\right)\left[\frac{\partial}{\partial \xi}\left(J^{\frac{1}{2}}\overline{V}\right)+\frac{\partial}{\partial \eta}\left(J^{\frac{1}{2}}\overline{U}\right)\right]. \tag{21}$$

In the turbulent energy equation we retain the assumptions previously made but now compute $\overline{u'^2}$ and $\overline{v'^2}$ from equation (19). We also include horizontal diffusion given by

$$\overline{u'p'}+\overline{u'E'}=-J^{\frac{1}{2}}K_E\left(\partial \overline{E}/\partial \xi\right). \tag{22}$$

With the new scheme we are able to allow full correction for the use of upstream differences. Surface shear and normal stress ($\bar{p}+\bar{v}'^2$) results for the case $a/z_0 = 250$, $L/z_0 = 10\,000$, are shown in Fig. 10 and compared with the predictions of the earlier model. Note that at the surface $\bar{v}'^2 = (2E/3)$ and so the normal stress is simply $\overline{p^{**}}$. There are some differences in this case between the predictions in that surface shear stresses are slightly lower and there is a compensatory shift in the phase of the surface pressure maximum. This is reflected by a change in the contribution of form drag (due to the pressure forces) to the total horizontal stress on the bed from 22 per cent with the original model to 26 per cent with the isotropic eddy viscosity model. The most pronounced changes occur in the magnitudes of the elevated stress extrema as a result of the change in the expression used for shear stress. This can be seen in Table 4 which shows the pressure and shear stress extrema both for these cases and for the case with $a/z_0 = 400$. One of the main motivations for developing this isotropic or scalar eddy viscosity model was to enable us to carry out the numerical experiments described in the next section.

## 9. Streamline curvature effects

Bradshaw (1973) has recently reviewed the effects of streamline curvature on turbulent flow and draws particular attention to the influence of ' extra ' rates of strain (e.g. $(\partial \overline{V}/\partial x)$ compared to $(\partial \overline{U}/\partial y)$) on the structure of the turbulence. These effects can be incorporated empirically into our model in a rather tentative way by making use of the curvature-buoyancy analogy described by Bradshaw. To achieve this we assume that our length scales $l$, $l_D$ are modified so that, with curvature effects,

$$`l' = lF(\text{` Rf '}).$$

Here, ' Rf ' is the curvature analogue of the flux Richardson number. In meteorological terms $F = \Phi^{-1}$, where $\Phi$ is the dimensionless wind shear (see Monin & Yaglom 1971). A relatively simple form for $F$ is:—

$F = 1-\alpha$ ' Rf ' for ' Rf ' $< 0$ (Analogous to statically unstable situations)

$$F = (1+\alpha \text{ ' Rf '})^{-1} \text{ for ' Rf ' } > 0 \text{ (Stable situations).} \tag{23}$$

The value of $\alpha$ is somewhat uncertain but the buoyancy analogue would indicate a value of about 5, while Bradshaw suggests 10. The definition of ' Rf ' is not entirely

**Table 4**

*Stress extrema etc. with standard and 'isotropic K' models:* $(L/z_0) = 10\,000$

| | | $a/z_0 = 250$ Standard | $ak = 0{\cdot}157$ Isot. model | $a/z_0 = 400$ Standard | $ak = 0{\cdot}251$ Isot. model |
|---|---|---|---|---|---|
| $\langle\tau_{surf}\rangle$ | | 0·78 | 0·74 | 0·54 | 0·48 |
| Surface shear stress | $\tau_{max}$ | 1·62 | 1·57 | 1·72 | 1·56 |
| | $\tau_{min}$ | 0·32 | 0·29 | 0·08 | 0·07 |
| | $\varepsilon^*$ | −22° | −22° | −19° | −18° |
| Elevated shear stress extrema | $\tau_{max}$ | 1·67 | 1·51 | 1·89 | 1·61 |
| | $\tau_{min}$ | 0·14 | 0·24 | −0·29 | −0·19 |
| Surface pressure field | $p_{max}$ | 22·7 | 21·5 | 22·3 | 20·0 |
| | $p_{min}$ | −36·1 | −34·4 | −47·3 | −42·2 |
| | $\varepsilon^*$ | 191° | 193° | 199° | 201° |

* $\varepsilon$ are phases (in $\xi$) of pressure and shear stress maxima relative to the crest of the underlying surface.

straightforward and we choose a form based on cartesian co-ordinates which differs by a factor of 2 from that adopted by Bradshaw. It is perhaps worth recalling that for stratified, rectilinear, shear flow 'Rf' is defined via the turbulent energy equation (e.g. Turner 1973) as the ratio of the rate of removal of turbulent kinetic energy ($\overline{v'^2}$ component) by working against buoyancy forces to the rate of production by the shear ($\overline{u'^2}$ component).

For unstratified curvilinear flow in cartesian co-ordinates the turbulent energy equation may be written

$$\frac{\partial \bar{E}}{\partial t} + \bar{U}\frac{\partial \bar{E}}{\partial x} + \bar{V}\frac{\partial \bar{E}}{\partial y} = -\overline{u'v'}\frac{\partial \bar{U}}{\partial y} - \overline{u'v'}\frac{\partial \bar{V}}{\partial x} - \overline{u'^2}\frac{\partial \bar{U}}{\partial x} - \overline{v'^2}\frac{\partial \bar{V}}{\partial y}$$

$$+ \text{Flux divergence} - \varepsilon. \qquad (24)$$

If the $x$ direction is aligned with the local mean flow then the second of the production terms on the right-hand side of this equation is directly associated with mean streamline curvature and the production of $\frac{1}{2}\overline{v'^2}$ while the last two production terms could perhaps be associated with extra rates of strain due to streamwise convergence or divergence effects. We can choose to define

$$\text{'Rf'} = -\left(\frac{\partial \bar{V}}{\partial x}\right)\Big/\left(\frac{\partial \bar{U}}{\partial y}\right).$$

If, as may well be the case, the flow is not aligned with the axes there may be a contribution to $(\partial\bar{V}/\partial x)$ not associated with streamline curvature. This can be partially corrected for if we define

$$\text{'Rf'} = -\left(\frac{\partial \bar{V}}{\partial x} - \frac{\bar{V}}{\bar{U}}\frac{\partial \bar{U}}{\partial x}\right)\Big/\left(\frac{\partial \bar{U}}{\partial y}\right). \qquad (25)$$

In the case of our curvilinear co-ordinates there will be extra contributions associated with the curvature of the co-ordinate system (see equation (13)). The extra production of $(\overline{v'^2}/2)\,J^{-\frac{1}{2}}$ may be written as

$$\frac{J_\xi}{2J}\left[\bar{U}\,\overline{v'^2} + \overline{u'v'}\,\bar{V}\right] - \frac{J_\eta}{2J}\left[2\bar{U}\,\overline{u'v'}\right]$$

while the extra contribution to $(\overline{u'^2}/2)\,J^{-\frac{1}{2}}$ is

$$\frac{J_\eta}{2J}\,[\overline{U}\,\overline{u'v'}+V\,\overline{u'^2}]-\frac{J_\xi}{2J}\,[2\,\overline{V}\,\overline{u'v'}].$$

Thus in addition to production of turbulent energy associated with extra rates of strain introduced by streamline curvature there is some transfer between one component and another associated with the curvilinear nature of the co-ordinate system. We choose to exclude the latter in our definition of ' Rf ' and also, at this stage, to neglect some terms involving $\overline{V}$ in comparison to $\overline{U}$. The term $\overline{U}\,\overline{v'^2}\,(J_\xi/2J)$ above is regarded as a convergence effect and our definition of ' Rf ' becomes

$$\text{' Rf '} = -\left(\frac{\partial \overline{V}}{\partial \xi}-\frac{\overline{V}}{\overline{U}}\,\frac{\partial \overline{U}}{\partial \xi}+\frac{\overline{U}J_\eta}{2J}\right)\Big/\frac{\partial \overline{U}}{\partial \eta}. \tag{26}$$

These modifications to the mixing and dissipation lengths have been added to our isotropic eddy viscosity model and computations made for a range of values of $\alpha$; results for $\alpha = 5$ will be presented here. Surface stress results are shown in Fig. 10 and can be compared with the results from the isotropic model without curvature effects. There are no very dramatic changes in these surface shear stress distributions but we may note some reduction in peak shear stress over the crest, where ' Rf ' $> 0$. This reduces the contribution of shear stress to total horizontal stress on the bed from 74 to 69 per cent. As with thermal stratification effects the importance of streamline curvature becomes more pronounced as we move further from the wall. The elevated shear stress extrema are modified from $0{\cdot}24\,u_0^2$ and $1{\cdot}51\,u_0^2$, with $\alpha = 0$, to $0{\cdot}01\,u_0^2$ and $2{\cdot}21\,u_0^2$, with $\alpha = 5{\cdot}0$ and occur slightly further from the wall. Turbulent energy levels are similarly affected with a drop in the elevated minimum from $3{\cdot}04\,u_0^2$ to $1{\cdot}91\,u_0^2$—this minimum occurring at about $0{\cdot}14\,L$ downstream of the crest and a height of about $0{\cdot}024\,L$ in both cases. Values of ' Rf ' attained range from $-0{\cdot}20$ to $0{\cdot}58$ when $\alpha$ is set equal to zero, i.e. curvature effects are not operative. With $\alpha = 5$ the range increases to $-0{\cdot}23$ to $0{\cdot}89$ implying that the inclusion of these effects in the closure hypotheses increases streamline curvature for this flow. These ' Rf ' maxima and minima occur more or less directly above the crest and trough respectively at heights of about $0{\cdot}1\,L$ and $0{\cdot}17\,L$. With the extremely low values of shear stress and of $(\partial U/\partial \eta)$ encountered at the elevated minima we are probably stretching our definition of ' Rf ' (equation (25)) and form for $F$ (equation (23)) to the limit. With this reservation we can state that, for this flow, modification of the closure hypotheses to include curvature effects gives rise to significant changes in predicted values for shear stress etc. away from the wall but to relatively small changes in predicted surface stresses. There are no qualitative changes in the overall flow pattern.

## 10. Conclusions

The study described here is, conceptually if not chronologically, the first of a series of numerical investigations of turbulent boundary-layer flow above 'gentle topography'. An essential feature is the treatment of the full non-linear problem in contrast to other semi-analytic treatments (e.g. Townsend 1972). A further study, Taylor & Gent (1974), presents some preliminary results on atmospheric boundary-layer flow over hills and, in addition, work is under way on flow above moving wavy surfaces for application to the study of wind wave generation. The models described here have evolved over three or four years during which several alternatives have been discarded. A few results from one of the earlier models are given in Taylor (1974).

The immediate application of the present work is to the study of flow and the associated sediment transport rates over sand or gravel waves in conditions under which mean flow separation does not occur. Some tentative attempts to predict local bed load transport rates using results obtained with the models presented here are described by Taylor & Dyer (1975) and a thorough investigation of the implications of the present work for sediment transport is planned for the near future. It is hoped that this work may stimulate more detailed observations of non-separating flow over sand waves both in flumes and on the sea bed. In conjunction with high quality observations of this type it should be possible to improve our understanding of the factors affecting the formation and growth of sand waves and the prediction of sediment transport rates associated with their movement.



**Acknowledgments**

The incentive for this investigation came from Dr K. R. Dyer (Institute of Oceanographic Sciences, Taunton) and his studies of flow over sand and gravel waves in the Solent. A considerable amount of preliminary work was undertaken while one of the authors (PAT) was a summer visitor with the Danish Atomic Energy Commission at Research Establishment Risø (1972). The research has been supported by the Natural Environment Research Council (UK) under grant GR3/1932.

*Department of Oceanography,*
*University of Southampton,*
*Southampton, SO9 5NH*

## References

Benjamin, T. B., 1959. Shearing flow over a wavy boundary. *J. fluid Mech.* **6,** 161–205.

Bradshaw, P., 1973, Effects of streamline curvature on turbulent flow, *AGARDograph* 169, *NATO*, Paris, 80 pp. plus appendices and figures.

Busch, N. E., 1973. On the mechanics of atmospheric turbulence, in *Workshop on micrometeorology*, ed. D. A. Haugen, American Meteorological Society, Boston.

Chorin, A. J., 1957. A numerical method for solving incompressible viscous flow problems, *J. comp. Phys.*, **2,** 12–26.

Dyer, K. R., 1970. Current velocity profiles in a tidal channel, *Geophys. J. R. astr. Soc.*, **22,** 153–161.

Hino, M., 1968. Computer experiment on smoke diffusion over a complicated topography, *Atmospheric Environment* **2,** 541–558.

Hinze, J. O., 1959. *Turbulence*, McGraw–Hill, New York, 586 pp.

Hsu, S-T & Kennedy, J. F., 1971. Turbulent flow in wavy pipes, *J. fluid Mech.*, **47,** 481–502.

Kendall, J. M., 1970. The turbulent boundary-layer over a wall with progressive surface waves, *J. fluid Mech.*, **41,** 259–281.

Long, R. B., 1971. *On generation of ocean waves by a turbulent wind*, PhD Thesis, U. of Miami, Florida.

Monin, A. S. & Yaglom, A. M., 1971. *Statistical fluid mechanics, vol. I.*, (English translation) M.I.T. Press, Cambridge, Mass., 769 pp.

Motzfeld, H., 1937. Die turbulente Strömung an welligen Wänden, *Z. angew. Math. Mech.*, **17,** 193–212.

Neumann J. & Mahrer, Y., 1971, A theoretical study of the land and sea breeze circulation, *J. atmos. Sci.*, **28,** 532–542.

Onishi, G. & Estoque, M. A., 1968. Numerical study on atmospheric boundary–layer flow over inhomogeneous Terrain, *J. Met Soc. Japan.*, **46,** 280–285.

Paskonov, V. M. & Soprunenko, I. P., 1963, Boundary-layer on a slightly wavy wall, in *Numerical methods in Gas Dynamics* ed. G. S. Roslyakov and L. A. Chudov, Moscow State University—translation by Israel Program for Scientific Translations, Jerusalem (1966).

Shir, C. C., 1972. A numerical computation of air flow over a sudden change of surface roughness, *J. atmos. Sci.*, **29**, 304–310.

Taylor, P. A., 1973. Some comparisons between mixing-length and turbulent energy equation models of flow above a change in surface roughness, *Lecture Notes in Physics* **19**, 246–253 (Springer, Berlin).

Taylor, P. A., 1974. Urban meteorological modelling—some relevant studies, *Adv. Geophys.*, **18B**, 173–186.

Taylor, P. A. & Dyer, K. R., 1975. Theoretical models of flow near the bed and their implications for sediment transport, *The Sea; Ocean Models*, vol. VI. in press.

Taylor, P. A. & Gent, P. R., 1974. A model of atmospheric boundary-layer flow above an isolated two dimensional " hill "; an example of flow above " gentle topography ". *Boundary-layer Meteorol.* **7**, 349–362.

Townsend, A. A., 1972. Flow in a deep turbulent boundary-layer over a surface distorted by water waves, *J. fluid Mech.*, **55**, 719–735.

Turner, J. S., 1973. *Buoyancy effects in fluids*, Cambridge University Press, 367 pp.

Ursell, F., 1956, Wave generation by wind, in *Survey in mechanics*, eds., G. K. Batchelor and R. M. Davies, Cambridge University Press.

## Appendix

### Numerical methods

In this appendix we wish to briefly describe the numerical methods used to obtain the solutions given. The iterative technique used is rather unusual but of limited interest as it is only stable for non-separating flow.

With the hypotheses stated in Section 3 the equations we wish to solve may be non-dimensionalized wrt $u_0$ and $z_0$, transferred to $(\xi, \zeta)$ co-ordinates (see equations (16)), and written, for the TE model, as

$$\bar{U}\frac{\partial \bar{U}}{\partial \xi} + e^{-\zeta}\bar{V}\frac{\partial \bar{U}}{\partial \zeta} = \frac{1}{2J}(J_\eta \bar{U}\bar{V} - J_\xi \bar{V}^2) - \frac{\partial \bar{p}}{\partial \xi} - 0{\cdot}65\frac{\partial \bar{E}}{\partial \xi} + e^{-\zeta}\frac{\partial}{\partial \zeta}\left(l(\lambda \bar{E})^{\frac{1}{2}} e^{-\zeta}\frac{\partial}{\partial \zeta}(J^{\frac{1}{2}}\bar{U})\right) + \frac{1}{2J}(0{\cdot}65\bar{E}J_\xi - 2\tau J_\eta), \tag{A1}$$

$$\bar{U}\frac{\partial \bar{V}}{\partial \xi} + e^{-\zeta}\bar{V}\frac{\partial \bar{V}}{\partial \zeta} = \frac{1}{2J}(J_\xi \bar{U}\bar{V} - J_\eta \bar{U}^2) - \frac{\partial \bar{p}}{\partial \eta} + \frac{\partial \tau}{\partial \xi} + \frac{1}{2J}(-0{\cdot}65\bar{E}J_\eta - 2\tau J_\xi), \tag{A2}$$

$$\frac{\partial}{\partial \xi}(J^{-\frac{1}{2}}\bar{U}) + \frac{\partial}{\partial \eta}(J^{-\frac{1}{2}}\bar{V}) = 0. \tag{A3}$$

and

$$\bar{U}\frac{\partial \bar{E}}{\partial \xi} + e^{-\zeta}\bar{V}\frac{\partial \bar{E}}{\partial \zeta} = \frac{J_\eta}{2J}(1{\cdot}0\,\bar{E}\bar{V} + \tau\bar{U}) + \frac{J_\xi}{2J}(0{\cdot}35\,\bar{E}\bar{U} + \tau\bar{V})$$

$$+\tau\left(e^{-\zeta}\frac{\partial \bar{U}}{\partial \zeta} + \frac{\partial \bar{V}}{\partial \xi}\right) - 1{\cdot}0\,\bar{E}\frac{\partial \bar{U}}{\partial \xi} - 0{\cdot}35\,\bar{E}\,e^{-\zeta}\frac{\partial \bar{V}}{\partial \zeta}$$

$$-J^{+\frac{1}{2}}e^{-\zeta}\frac{\partial}{\partial \zeta}\left[e^{-\zeta}K_E\frac{\partial \bar{E}}{\partial \zeta}\right]$$

$$-J^{-\frac{1}{2}}\bar{E}^{3/2}/l_D. \qquad \text{(A4)}$$

In equation (A1) we make use of the stress-strain closure hypothesis (equation (10)) to express the term $e^{-\zeta}(\partial\tau/\partial\zeta)$ in terms of $\bar{U}$ derivatives.

In other places where $\tau$ appears the latest estimate (in the iteration cycle to be described) is used.

Some derivatives are left in terms of $\eta$ in an attempt to minimize certain discretatisation errors when finite difference representations are used. These equations are to be solved in $0 \leqslant \xi \leqslant L$, $0 \leqslant \eta \leqslant H$ (or $0 \leqslant \zeta \leqslant \ln((H+z_0)/z_0)$) and in order to achieve this we make use of a finite difference mesh with uniform grid spacing in $\xi$ and $\zeta$. Each mesh cell will have $p$ defined at its centre and velocities at the sides as in Fig. A1 which shows the arrangement of cells within the solution region. $\bar{E}$ is defined at the same points as $\bar{U}$ and $\tau$ at the corners of the grid cells. For the results presented a $20 \times 14$ cell grid was used although almost equally good results could be obtained with a $10 \times 10$ grid.

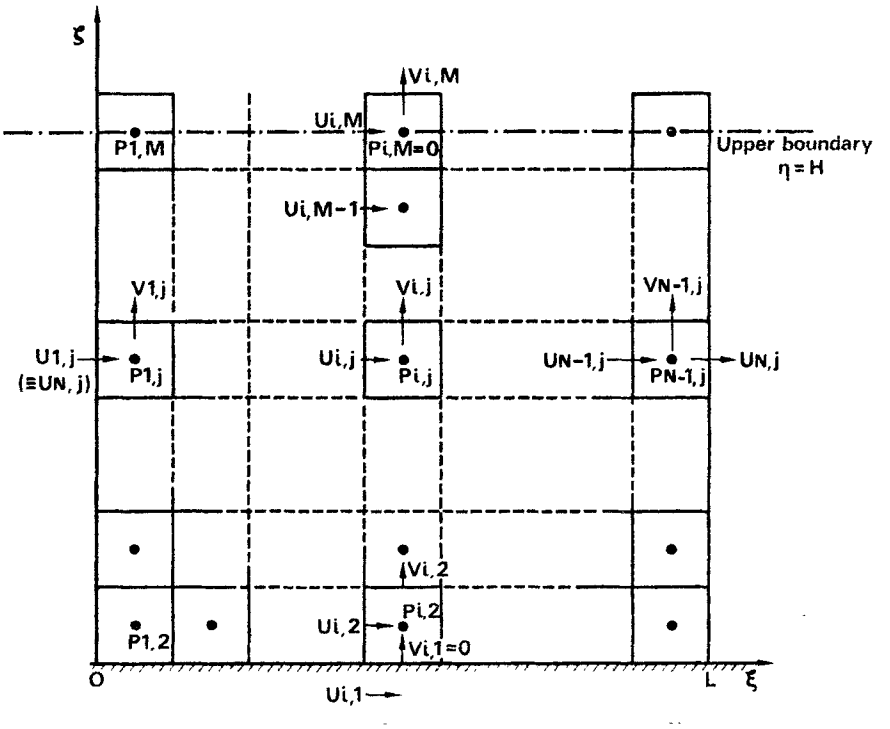


FIG. A1. Finite difference grid.

Equations (A1)–(A4) are expressed in finite difference form with equations (A1) and (A4) applied at points where $\overline{U}_{ij}$ is defined, (A2) at points where $\overline{V}_{ij}$ is defined and (A3) used as a finite difference representation of continuity within each cell. Straightforward central differences are used for all derivatives except the $\overline{U}(\partial/\partial\xi)$ terms where in the first instance upstream differences were used. As is well known these allow errors of $0(\Delta\xi)$ and we found that we could only satisfy overall momentum budgets to within about 7 per cent with upstream differences. In order to reduce this error a partial correction was made in which the $\overline{U}\,(\partial/\partial\xi)$ terms were represented by upstream differences on the LHS of equations (A1), (A2) and (A4) but correction terms, e.g. $-(C/2)\,|\overline{U}_{ij}|(\overline{U}_{i+1,j}-2\overline{U}_{ij}+\overline{U}_{i-1,j})/\Delta\xi$ in equation (A1), were added to the right-hand sides with $0 \leqslant C \leqslant 1$. A value $C = 1$ corresponds to a central difference scheme. We were able to achieve stability in a typical case for $C \leqslant 0{\cdot}98$ ($20 \times 14$ grid) and, in general, computations were made with $C = 0{\cdot}97$. The effect of this correction term can be seen in Fig. A2 where results for surface shear stress and pressure for our typical case are shown with 0, 50 per cent and 97 per cent correction. The peak shear stress values appear to suffer most from the errors introduced by upstream differences. The horizontal momentum balance has errors of $-7{\cdot}3$, $-3{\cdot}8$ and $+0{\cdot}5$ per cent in the three cases. Extrapolation, from for example 97 and 98 per cent to 100 per cent correction can be made but it produced negligible changes and was not considered worthwhile.

In order to solve the finite difference forms of equations (A1) –(A4) two different techniques were tried. The more economical of these we term the DIRECT method. It was tried somewhat arbitrarily and with little real hope of success. Somewhat to our surprise we found it a relatively efficient method for this particular problem.

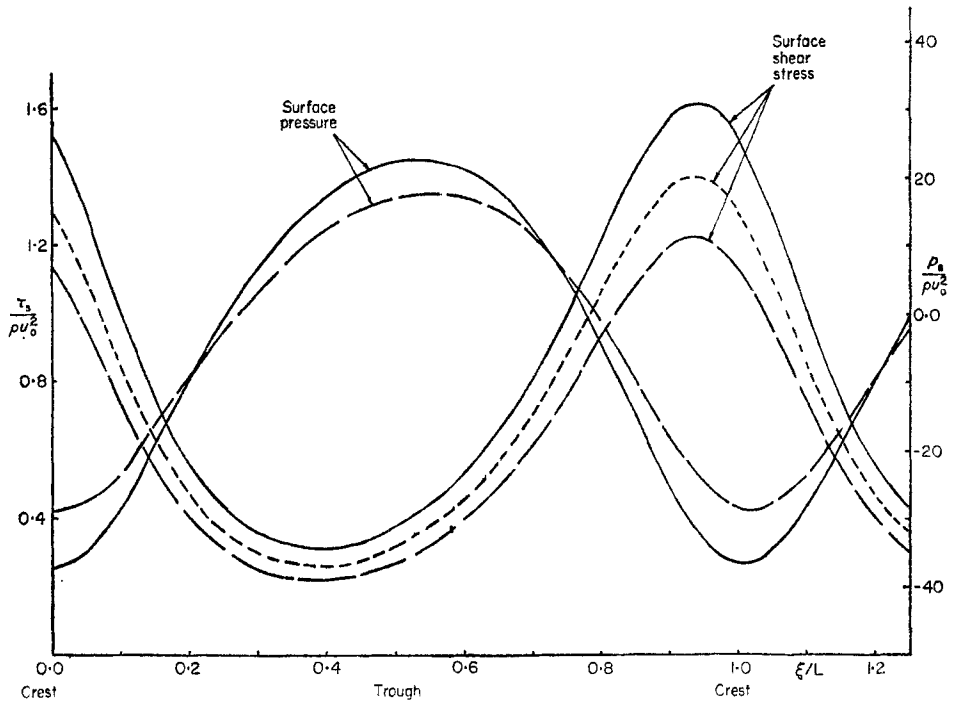


FIG. A2. The effect of correction for upstream differences. $L/z_0 = 10\,000$; $ak = 0{\cdot}157$, —— 97 per cent correction; – – – 50 per cent correction; — – — – no correction.

The procedure is as follows:

(1) Guess initial $U^0$, $V^0$, $E^0$ and $p^0$ fields—usually $u_0\,\zeta/\kappa$, 0, ${u_0}^2/\lambda$, 0.

(2) Compute new $U$ and $E$ fields, $U^1$, $E^*$ from the finite difference representations of equations (A1), (A4) marching from left to right ($I = 2, 3, \ldots N$) and solving, column by column in a block iterative fashion. A stress field is then computed and relaxation applied on the $E$ and $\tau$ fields to give $E^1$ and $\tau^1$. No relaxation is applied to $U$.

(3) Use $U^1$ in the finite difference representation of the continuity equation and column by column integrate upwards from $\zeta = 0$ to obtain a new $V$ field, $V^*$. Relaxation is applied to the $V^*$ field and we set $V^1 = \alpha V^* + (1-\alpha)\,V^0$.

(4) Use the $V$ momentum equation (A2) to compute a new pressure field, $p^*$, by integrating downwards from $\eta = H$, where $p = 0$, again column by column and marching left to right. Relaxation is again applied. The same relaxation parameter being used.

(5) Cycle back to step (2) and continue, usually for about 3000 iteration cycles with a very low value of the relaxation parameter, (typically $\alpha^2 = 0{\cdot}001$).

Without relaxation this iteration is basically divergent and any disturbance of the type $p^0 = A\exp(ik\xi + il\eta)$ will be rapidly amplified, the amplification factor ($< 0$) being largest for $l = \pi/H$ (lower values of $l$ are not permitted by the boundary conditions) and the highest wavenumber, $k$, that can be represented by the finite difference mesh. The amplification factor is however negative provided $U > 0$ and the iteration can be made to converge with suitable relaxation. This does necessitate very low values of the relaxation parameter and large numbers of iteration cycles but we have found this approach more efficient for our particular problem than a method based on Chorin's (1967) 'artificial compressibility technique' with time derivatives introduced into the equations. Both methods gave essentially the same results in comparisons made on $10 \times 10$ grid schemes. Typical computation times for the $20 \times 14$ grid were approximately 60 s on a CDC 7600 computer using an optimized FORTRAN compiler.

Convergence was assessed somewhat subjectively and results accepted if they altered by less than 1 per cent between the 2000th and 3000th iteration cycles. An overall stress or momentum balance test was also applied as a check on convergence and discretization errors by computing the average horizontal force on the lower surface due to shear stresses and normal pressures. This should be equal to ${u_0}^2$. In the results to be presented agreement was achieved to within about 1 per cent. Checks were also made on the accuracy to which continuity was satisfied and that $\overline{V} \simeq 0$ at the upper boundary. The iteration scheme described here breaks down if the velocity becomes negative (giving a positive amplification factor for periodic disturbances) and in any extension of the work a different technique will have to be used.